JCI The Journal of Clinical Investigation

NOTCH inhibits osteoblast formation in inflammatory arthritis via noncanonical NF-κB

Hengwei Zhang, … , Brendan F. Boyce, Lianping Xing

J Clin Invest. 2014. https://doi.org/10.1172/JCI68901.

Research Article **Bone biology**

NOTCH-dependent signaling pathways are critical for normal bone remodeling; however, it is unclear if dysfunctional NOTCH activation contributes to inflammation-mediated bone loss, as observed in rheumatoid arthritis (RA) patients. We performed RNA sequencing and pathway analyses in mesenchymal stem cells (MSCs) isolated from transgenic *TNF*-expressing mice, a model of RA, to identify pathways responsible for decreased osteoblast differentiation. 53 pathways were dysregulated in MSCs from RA mice, among which expression of genes encoding NOTCH pathway members and members of the noncanonical NF-κB pathway were markedly elevated. Administration of NOTCH inhibitors to RA mice prevented bone loss and osteoblast inhibition, and CFU-fibroblasts from RA mice treated with NOTCH inhibitors formed more new bone in recipient mice with tibial defects. Overexpression of the noncanonical NF-κB subunit p52 and RELB in a murine pluripotent stem cell line increased NOTCH intracellular domain–dependent (NICD-dependent) activation of an RBPjκ reporter and levels of the transcription factor HES1. TNF promoted p52/RELB binding to NICD, which enhanced binding at the RBPjκ site within the *Hes1* promoter. Furthermore, MSC-enriched cells from RA patients exhibited elevated levels of HES1, p52, and RELB. Together, these data indicate that persistent NOTCH activation in MSCs contributes to decreased osteoblast differentiation associated with RA and suggest that NOTCH inhibitors could prevent inflammation-mediated bone loss.

NOTCH inhibits osteoblast formation in inflammatory arthritis via noncanonical NF-κB

Hengwei Zhang,[1] Matthew J. Hilton,[2] Jennifer H. Anolik,[3] Stephen L. Welle,[4] Chen Zhao,[1] Zhenqiang Yao,[1] Xing Li,[1,5] Zhiyu Wang,[5] Brendan F. Boyce,[1,2] and Lianping Xing[1,2]

[1]Department of Pathology and Laboratory Medicine, [2]Center for Musculoskeletal Research, [3]Division of Allergy/Immunology and Rheumatology, Department of Medicine, and [4]Functional Genomics Center, University of Rochester Medical Center, Rochester, New York, USA. [5]Department of Cancer Immunotherapy, The Fourth Hospital of Hebei Medical University, Shijiazhuang, People's Republic of China.

NOTCH-dependent signaling pathways are critical for normal bone remodeling; however, it is unclear if dysfunctional NOTCH activation contributes to inflammation-mediated bone loss, as observed in rheumatoid arthritis (RA) patients. We performed RNA sequencing and pathway analyses in mesenchymal stem cells (MSCs) isolated from transgenic *TNF*-expressing mice, a model of RA, to identify pathways responsible for decreased osteoblast differentiation. 53 pathways were dysregulated in MSCs from RA mice, among which expression of genes encoding NOTCH pathway members and members of the noncanonical NF-κB pathway were markedly elevated. Administration of NOTCH inhibitors to RA mice prevented bone loss and osteoblast inhibition, and CFU-fibroblasts from RA mice treated with NOTCH inhibitors formed more new bone in recipient mice with tibial defects. Overexpression of the noncanonical NF-κB subunit p52 and RELB in a murine pluripotent stem cell line increased NOTCH intracellular domain–dependent (NICD-dependent) activation of an RBPjκ reporter and levels of the transcription factor HES1. TNF promoted p52/RELB binding to NICD, which enhanced binding at the RBPjκ site within the *Hes1* promoter. Furthermore, MSC-enriched cells from RA patients exhibited elevated levels of HES1, p52, and RELB. Together, these data indicate that persistent NOTCH activation in MSCs contributes to decreased osteoblast differentiation associated with RA and suggest that NOTCH inhibitors could prevent inflammation-mediated bone loss.

Introduction

Patients with chronic inflammatory diseases, such as rheumatoid arthritis (RA), often have severe systemic bone loss and increased risk of fracture due to increased bone resorption and decreased bone formation, partially mediated by elevated TNF levels (1). We (1–4) and others (5, 6) have reported that TNF inhibits bone formation by affecting major osteoblast regulatory pathways, including BMP/SMAD/RUNX2 and WNT–β-catenin, but the role of TNF in osteoblast differentiation from MSCs has not been fully defined. The TNF transgenic (TNF-Tg) mouse model we use, line 3647, represents a good model of RA to study the influence of chronically elevated, but relatively low, levels of TNF and TNF-induced inflammation on bone cell function and MSC differentiation into osteoblasts (7). To attempt to identify molecules responsible for reduced differentiation of MSCs into osteoblasts in RA, we performed genome-wide screening and pathway analyses using data from RNA sequencing (RNA-Seq) of MSCs purified from TNF-Tg mice and WT littermates. We found that genes in the NOTCH and noncanonical NF-κB signaling pathways were markedly upregulated in TNF-Tg mouse MSCs, raising the possibility that NOTCH may interact with noncanonical NF-κB proteins in MSCs to inhibit their osteogenic differentiation.

NOTCH is a family of evolutionarily conserved receptors that regulate cell fate. NOTCH receptors are activated following direct contact with their ligands expressed on adjacent cells. In mammals, there are 4 NOTCH receptors (NOTCH1–NOTCH4) and 5 ligands (Jagged-1 [JAG1], JAG2, and Delta-like 1, 3, and 4). NOTCH receptors have extracellular, transmembrane, and intracellular domains. Upon ligand binding, the NOTCH intracellular domain (NICD) of the receptor is cleaved by γ-secretase and translocates to the nucleus, where it associates with the recombination signal–binding protein jκ (RBPjκ). RBPjκ is a key transcription factor in canonical NOTCH signaling and acts downstream of all 4 NOTCH receptors. In the absence of a NOTCH signal, RBPjκ inhibits transcription of target genes by binding to transcriptional corepressors. Following NOTCH activation, NICD binds to RBPjκ and displaces corepressors, leading to transcriptional activation of target genes such as *Hes1* and *Hey1*. Ligand binding also can lead to noncanonical NOTCH signaling, which is mediated through the interaction of NICD with factors other than RBPjκ to activate alternative signaling events.

Involvement of NOTCH in bone cells has been recognized since 2008 (8), when in vivo studies of genetically modified mice demonstrated that loss of NOTCH signaling in mesenchymal stem cells (MSCs) or osteoblast precursors resulted in increased bone mass (9, 10), whereas activation of NOTCH signaling decreased osteoblast numbers (11). NOTCH signaling maintains MSCs in a proliferative phase and inhibits osteoblast differentiation. NOTCH also inhibits osteoclast formation via indirect and direct mechanisms. Depletion of NOTCH (11) or γ-secretase (9) in osteoblasts decreased osteoprotegerin production, leading to increased osteoclast formation, whereas RBPjκ depletion specifically in myeloid cells increased osteoclast formation in response to inflammatory cytokines (12). Although a role for NOTCH signaling in MSC and osteoblast differentiation has been described in normal mice, little is known about its role or the effects of NOTCH inhibitors in these cells in common bone diseases, such as RA.

NF-κB is a family of transcription factors that regulate many aspects of normal cellular functions as well as innate and adaptive immunity in response to pathogens and autoimmune

Conflict of interest: The authors have declared that no conflict of interest exists.
Citation for this article: *J Clin Invest.* doi:10.1172/JCI68901.

stimuli (13, 14). The family includes NF-κB1 (also known as p50, and its precursor p105), NF-κB2 (p52, and its precursor p100), RELA, RELB, and c-REL. Homo- and heterodimers of these proteins activate transcription of target genes, typically through canonical (p50/RELA) and noncanonical (p52/RELB) signaling. NF-κB signaling (which typically refers to canonical RELA-mediated transcription) regulates many aspects of cellular activity (15). *Rela*$^{-/-}$ mice die during embryonic development, making direct study of the role of RELA in bone difficult (16), although rescue studies indicate that RELA prevents osteoclast precursor apoptosis (17). Inhibition of RELA in mature osteoblasts by a dominant-negative IKK-γ mutant increases bone mass (18). Double-knockout *Nfkb1*$^{-/-}$ *Nfkb2*$^{-/-}$ mice are severely osteopetrotic because they have no osteoclasts (19). Double-knockout *Nfkb2*$^{-/-}$ *Relb*$^{-/-}$ mice (referred to herein as p52/RELB dKO mice) have increased bone volume (20, 21), a phenotype also seen in *Relb*$^{-/-}$ mice due to enhanced RUNX2 activation and osteoblast precursor differentiation (22). Despite these advances in understanding of the role of NF-κB in bone, the relative roles of canonical versus noncanonical signaling in MSC functions in RA have not been defined. To date, the only reported interaction between NOTCH and NF-κB was in cells in the hematopoietic lineage and cancer cells. Most of these studies suggested that NOTCH regulates the transcription of *Nfkb* (23, 24). They focused on canonical NF-κB signaling (25), and consequently, it is not known whether there is a relationship between NOTCH and noncanonical NF-κB signaling in bone cells.

In the present study, we found persistent activation of the NOTCH and noncanonical NF-κB pathways in MSCs and in MSC-enriched cells from TNF-Tg mice. Enhanced NOTCH signaling in MSCs was associated with reduced osteoblast differentiation and bone formation, which was prevented by systemic administration of the NOTCH inhibitors N-[N-(3,5-difluorophenacetyl)-l-alanyl]-S-phenylglycine t-butyl ester (DAPT) and thapsigargin. At the molecular level, we found that TNF increased expression of the noncanonical NF-κB proteins p52 and RELB, which potentiated NOTCH activation by binding to and promoting nuclear translocation of NICD onto the *Hes1* promoter. Thus, inhibition of NOTCH represents a potential new therapeutic approach for inflammatory bone loss when NOTCH is activated in MSCs.

Results

Increased expression of NOTCH target genes in MSCs from TNF-Tg mice and TNF-treated MSCs. BM MSCs from TNF-Tg mice with inflammatory arthritis have significantly decreased osteoblast differentiation potential (1). To identify the molecules and pathways responsible for TNF-induced inhibition of osteoblast differentiation, we purified MSCs (CD45$^-$CD105$^+$SCA1$^+$) from 6-month-old TNF-Tg mice (which typically have developed severe systemic bone loss by this age; ref. 1) and WT littermates by flow sorting, and performed RNA-Seq using a single-cell protocol. We identified 965 differentially expressed genes (>1.5-fold change; $P < 0.05$) between TNF-Tg and WT cells from a total of 21,533 reference genes (Figure 1A; RNA-Seq results available at the NCBI Sequence Read Archive; accession no. SRX543086) and submitted them to 2 different pathway analyses: Ingenuity Pathway Analysis (IPA) and David Bioinformatics Resources Program (David program), according to the Ingenuity Pathways Knowledge and KEGG databases, respectively. For all analyses, Fisher exact test was used to calculate a *P* value determining the probability that each pathway assigned to the data set was due to chance alone. IPA analysis revealed 53 dysregulated pathways between TNF-Tg and WT cells (Supplemental Figure 1A; supplemental material available online with this article; doi:10.1172/JCI68901DS1). Among them, the NOTCH signaling pathway was in 14th place of 53 dysregulated pathways identified from the IPA analysis and in 7th place of 11 dysregulated pathways from the David program (Supplemental Figure 1B).

NOTCH signaling molecules contain 4 mammalian NOTCH receptors (NOTCH1–NOTCH4), 5 ligands (JAG1 and JAG2 and Delta-like 1, 3, and 4), 2 inhibitors (NUMB and NUMBL), and 4 coactivators (DTX1–DTX4) (26). In MSCs, RNA-Seq detected various expression levels of these NOTCH-related genes (Supplemental Figure 2). Interestingly, despite different levels of upstream NOTCH signaling molecules in cells from TNF-Tg mice, expression levels of the NOTCH target genes *Hes1* and *Hey1* were increased, which was confirmed by quantitative real-time RT-PCR (qPCR) in purified CD45$^-$CD105$^+$SCA1$^+$ MSCs (Figure 1B). Increased *Hes1* and *Hey1* expression was also demonstrated by qPCR in various TNF-treated MSC preparations, including: (a) 3rd-passage bone-derived MSCs from WT mice (Figure 1C), which we characterized as cells expressing MSC surface markers (93% CD45$^-$, 70% CD105$^+$, 72% SCA1$^+$, 90% CD44$^+$) and able to differentiate to osteoblasts, adipocytes, and chondrocytes in vitro (Supplemental Figure 3); (b) the murine MSC line C3H10T1/2 (Figure 1D); and (c) human MSCs purchased from Lonza and characterized as CD105$^+$CD166$^+$CD29$^+$CD44$^+$CD14$^-$CD34$^-$CD45$^-$ (Figure 1E). In a prior study, we demonstrated that mouse MSCs express *Hes1* among other NOTCH targets and that HES1 mediates much of the NOTCH effect on MSC-osteoblast differentiation (10), which indicates that *Hes1* is an important NOTCH downstream gene in MSCs. Thus, in subsequent experiments, we used *Hes1* as a readout measure for NOTCH activation.

TNF signals through TNF receptor 1 (TNFR1) and TNFR2 (27). To determine whether TNF receptors mediate *Hes1* expression upregulated by TNF, we injected murine TNF (0.5 μg/injection/d i.p.) into double-knockout *Tnfr1*$^{-/-}$ *Tnfr2*$^{-/-}$ (TNFR1/2 dKO) mice and WT littermates for 5 days. We examined the expression level of *Hes1* in CD45$^-$ MSC-enriched cells and in CD45$^+$ non-MSCs by qPCR. TNF increased *Hes1* expression in WT CD45$^-$ cells, but not CD45$^+$ cells, and had no effect on CD45$^-$ or CD45$^+$ cells in TNFR1/2 dKO mice (Figure 1F). Accordingly, TNF decreased alkaline phosphatase–positive CFU-fibroblast (CFU-ALP$^+$) numbers in WT cells, but had no effect in TNFR1/2 dKO cells (data not shown).

Short-term Notch inhibition by DAPT reverses decreased osteoblast differentiation of MSCs from TNF-Tg mice. NOTCH controls the fate of MSCs, including their osteoblast differentiation potential (10). However, the role of NOTCH in common bone disorders, such as osteoporosis, has not been well investigated. NOTCH inhibitors have not been tested in mouse osteoporotic models, perhaps reflecting concerns that sustained inhibition of NOTCH in the BM may have adverse effects, such as increased bone resorption (12). To investigate whether NOTCH inhibition can reverse the suppressed osteoblast differentiation in TNF-Tg mice, we administered the γ-secretase inhibitor DAPT to TNF-Tg mice and WT littermates by gavage for 4 days. The inhibitory effects of DAPT on NOTCH signaling was confirmed by decreased *Hes1* mRNA levels in popliteal lymph nodes (Figure 2A), an indicator of effective NOTCH inhibition in vivo, but not in spleen (Supplemental Figure 4), as described previously (28). Interestingly, CD45$^-$ MSC-enriched

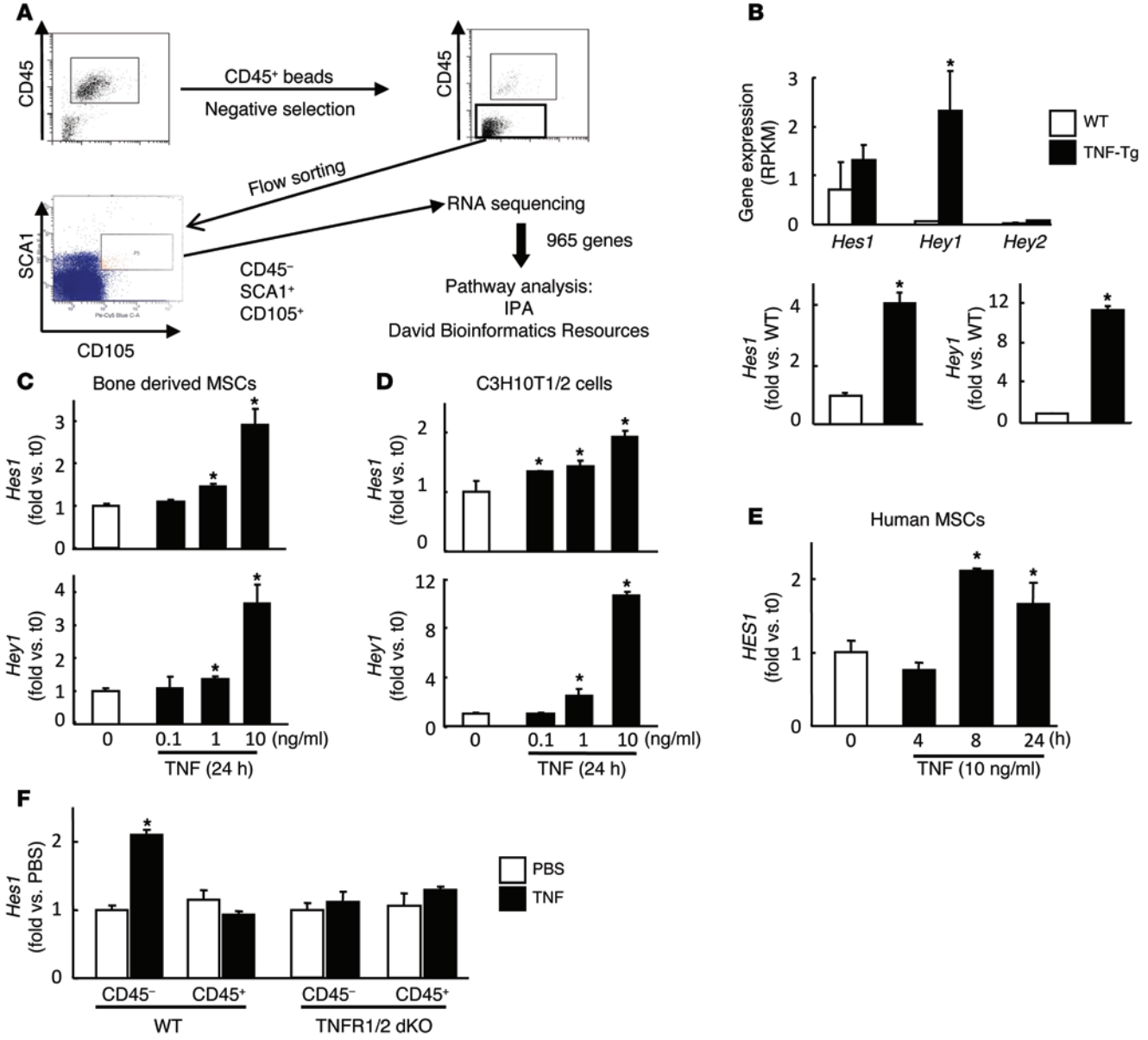

Figure 1

Increased expression of NOTCH target genes in MSCs from TNF-Tg mice and TNF-treated MSCs. (**A**) BM cells were isolated from 6-month-old TNF-Tg mice and WT littermates (n = 3 per genotype). CD45$^-$SCA1$^+$CD105$^+$ MSCs were subjected to RNA-Seq using a single-cell protocol. Differentially expressed genes between TNF-Tg and WT cells were subjected to pathway analysis. (**B**) RNA-Seq reads (top) and qPCR data (bottom) from CD45$^-$SCA1$^+$CD105$^+$ MSCs of TNF-Tg and WT mice. RPKM, reads per kilobase per million. (**C** and **D**) Expression of *Hes1* and *Hey1* in TNF-treated (24 hours) 3rd passage of bone-derived WT MSCs (**C**) and in the C3H10T1/2 murine MSC line (**D**) by qPCR. (**E**) Expression of *HES1* in TNF-treated (24 hours) human MSCs by qPCR. (**F**) 2-month-old TNFR1/2 dKO mice and WT littermates received TNF (0.5 μg/injection/d i.p.) or PBS for 5 days. BM cells were subjected to CD45$^-$ or CD45$^+$ cell isolation for *Hes1* expression by qPCR. *P < 0.05 vs. respective control.

cells from DAPT-treated WT mice had low levels of *Hes1* expression, similar to cells from vehicle-treated WT mice. CD45$^-$ MSC-enriched cells from vehicle-treated TNF-Tg mice had significantly increased *Hes1* levels compared with WT cells, and this was reduced by 50% in cells from DAPT-treated TNF-Tg mice (Figure 2B). To investigate whether DAPT affects osteoblastic differentiation of MSCs in TNF-Tg mice, we examined CFU-ALP$^+$ colony formation using BM stromal cells from DAPT- or vehicle-treated mice. As we previously reported (1), cells from TNF-Tg mice formed significantly decreased numbers of CFU-ALP$^+$ colonies compared with WT cells, an effect that was largely reversed with DAPT treatment. In contrast, CFU-ALP$^+$ colony numbers were similar in cells of DAPT- and vehicle- treated WT mice (Figure 2C).

To determine whether MSCs from DAPT-treated mice can form more new bone, and whether increased new bone formation is independent of the BM environment of TNF-Tg mice, we performed in vivo bone formation assays, as we described recently (22, 29), using cells from CFU mesenchymal colonies derived from

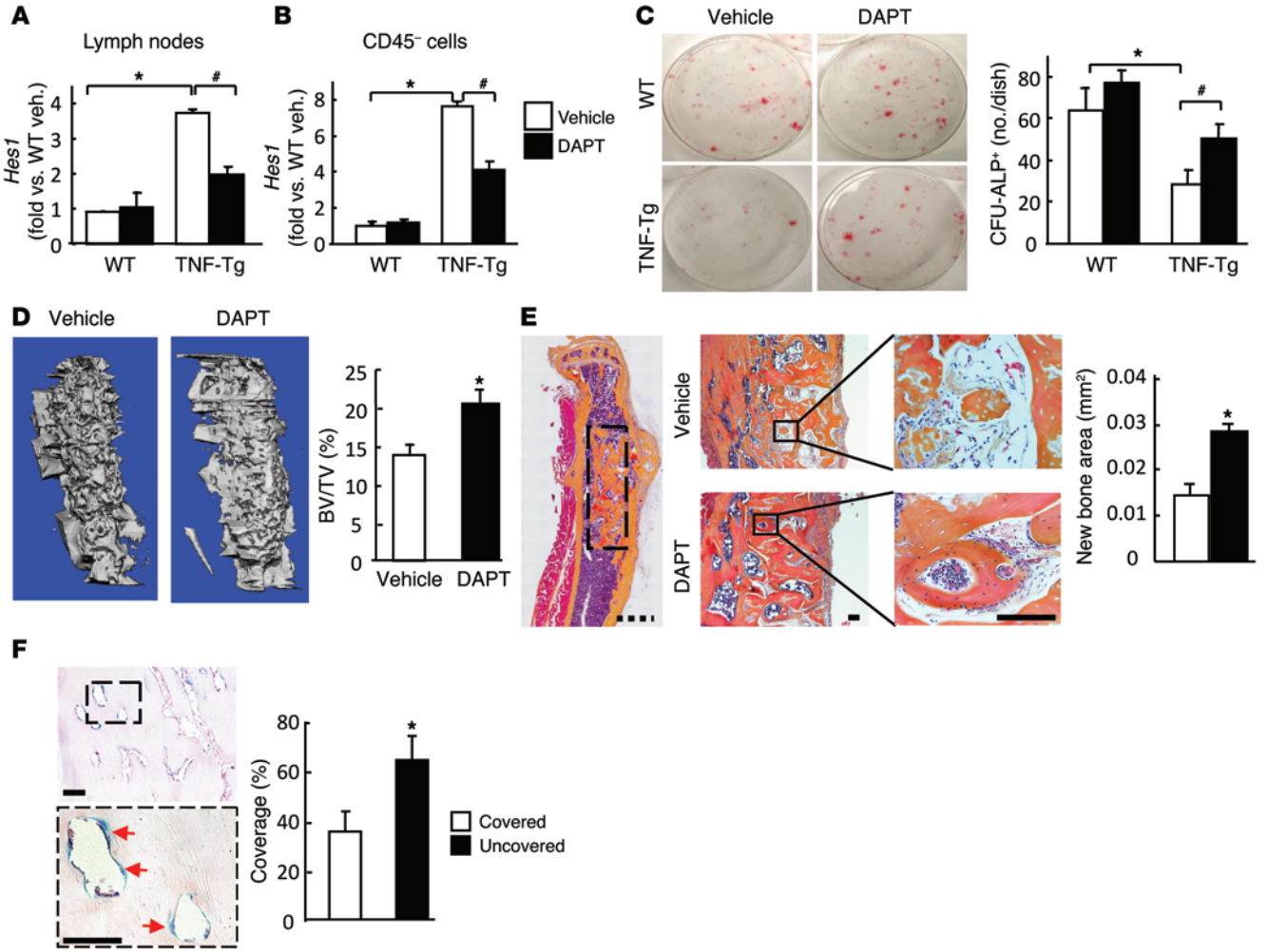

Figure 2

Short-term DAPT treatment revised decreased osteoblast differentiation of MSCs in TNF-Tg mice. (**A**–**C**) TNF-Tg mice and WT littermates were gavaged with DAPT (5 mg/kg each time) or vehicle daily for 4 days. The inhibitory effect of short-term DAPT treatment on NOTCH activation (*Hes1* mRNA) was confirmed in the popliteal lymph nodes (**A**; positive control) and in CD45⁻ MSC-enriched cells (**B**) by qPCR. (**C**) Representative images and number of CFU-ALP⁺ colonies in BM stromal cells. (**D** and **E**) CFU colony cells from vehicle- or DAPT-treated TNF-Tg mice were implanted to bone matrix in tibial cortical defects of SCID mice. Mice were sacrificed 6 weeks after surgery, and volume of new bone formed in the defects, relative to total defect volume (BV/TV), was measured by μCT (**D**), followed by histomorphometric analysis of the area of newly formed trabecular bone observed in decalcified H&E-stained bone sections (**E**). n = 8 per group. Scale bars: 1 mm (broken); 100 mm (solid). (**F**) CFU cells generated from BM stromal cells of *Rosa26-LacZ* mice were implanted to tibial cortical defects for 6 weeks as in **D**. Frozen sections were stained for LacZ enzymatic activity (blue) and counterstained with nuclear fast red (pink). Percent bone surface area covered by donor cells (LacZ⁺; red arrows) over total bone surface within the area of bone defect (green line) was assessed. n = 5 per group. Scale bars: 1 μm (broken); 100 μm (solid). *P < 0.05 vs. WT; #P < 0.05 vs. vehicle.

DAPT- or vehicle-treated TNF-Tg mice. We first demonstrated that a much higher percentage of CFU colony cells expressed MSC surface markers (50.4% CD45⁻, 89% SCA1⁺, 89% CD105⁺) compared with primary BM stromal cells (16% CD45⁻, 13% SCA1⁺, 7% CD105⁺) or freshly isolated BM cells (6% CD45⁻, 8% SCA1⁺, 2% CD105⁺) (Supplemental Figure 5). We loaded CFU colony cells from DAPT- or vehicle-treated TNF-Tg mice on decalcified bovine bone scaffolds and implanted them in tibial defects in recipient mice for 6 weeks. We examined the volume of newly formed bone by μCT and histomorphometric analysis and found that cells from DAPT-treated mice formed more new bone than cells from vehicle-treated mice (Figure 2, D and E).

To determine the fate of donor cells and their localization after they have been implanted in vivo for 6 weeks, we used CFU colony cells derived from *Rosa26-LacZ* mice in a separate experiment. LacZ⁺ cells were localized near the surfaces of newly formed bone, and they covered 37.3% of the total bone surface within the bone defect area (Figure 2F). To confirm that implanted MSCs were the major contributor to new bone formation, we compared mice that received only bone scaffolds with those that received bone scaffolds plus MSCs 6 weeks after implantation in WT mice (n = 5 per group). The implanting scaffold alone without MSCs could cause some degree of repair, perhaps via stimulation of MSCs from the host. However, the level of repair

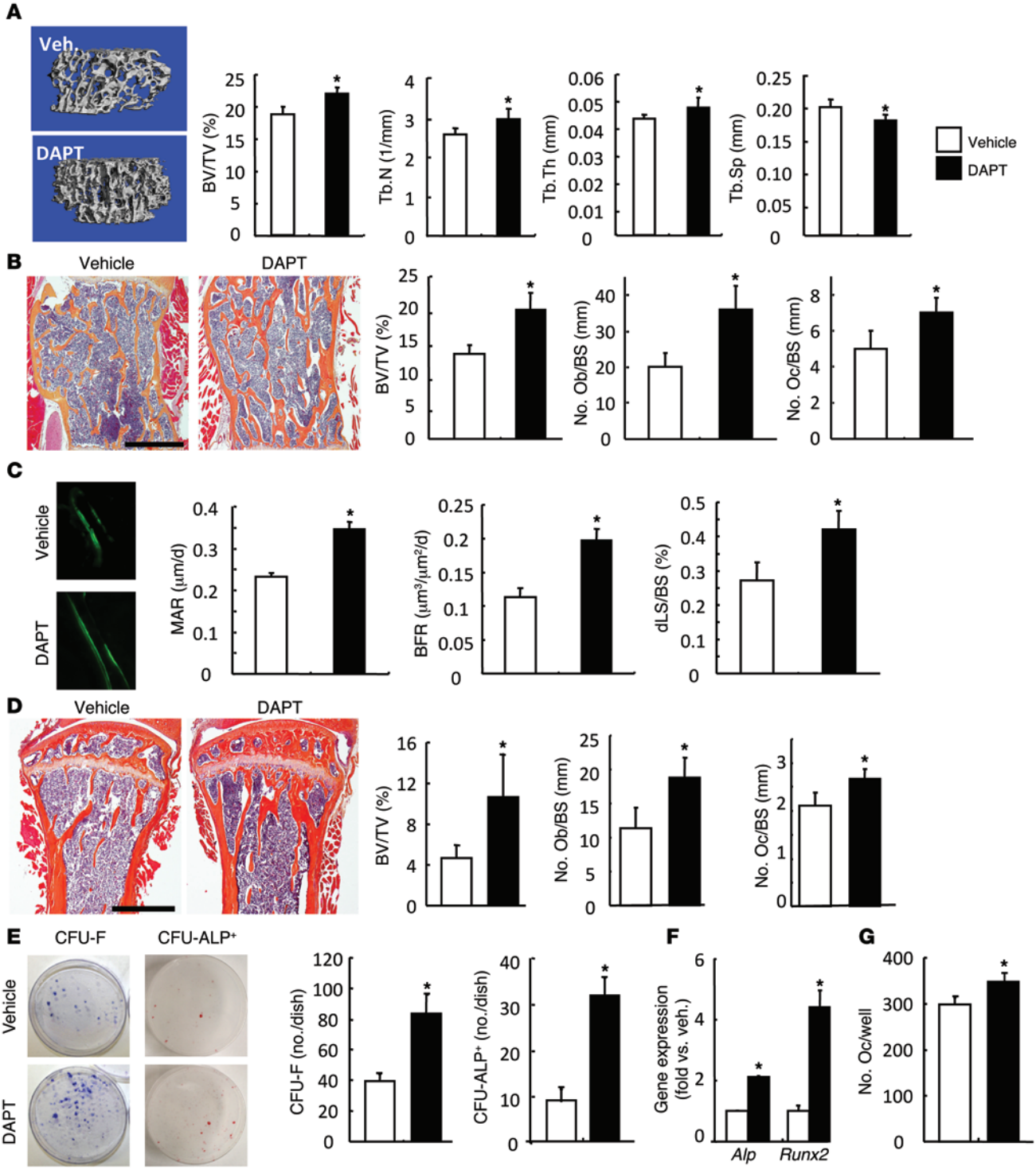

Figure 3

Long-term of DAPT treatment prevented bone loss in TNF-Tg mice. TNF-Tg mice were given with DAPT or vehicle as in Figure 2 for 3 months. (**A**) Representative μCT scans and morphometric data of BV/TV, trabecular number (Tb.N), trabecular thickness (Tb.Th), and trabecular separation (Tb.Sp) in L1 vertebrae. (**B**) Histology and histomorphometric analysis of BV/TV and number of osteoblasts (Ob) and osteoclasts (Oc) per bone surface (BS) in L1 vertebrae. (**C**) Calcein double-labeling in L1 vertebrae and analysis of dynamic parameters of bone formation: double labeled surface per bone surface (dLS/BS), mineral apposition rate (MAR), and bone formation rate (BFR). Original magnification, ×40. (**D**) Histology and histomorphometric analysis in the tibial metaphysis. Values are mean ± SD of 7–8 mice per group. (**E**) BM cells were cultured in the basal or osteoblast-inducing medium for 21 days in CFU colony formation assays. The number of CFU-F and CFU-ALP$^+$ colonies was evaluated. (**F**) Expression of *Alp* and *Runx2* in CFU-ALP$^+$ colonies, assessed by qPCR. (**G**) BM cells were cultured with RANKL and M-CSF for 5 days in osteoclastogenic assays. The number of TRAP$^+$ osteoclasts was counted. Values are mean ± SD of 4 dishes. Scale bars: 1 mm. *$P < 0.05$ vs. vehicle.

was much higher (5- to 6-fold) when MSCs were included along with scaffold (Supplemental Figure 6).

Long-term Notch inhibition by DAPT prevents bone loss in TNF-Tg mice. Patients and mice with inflammatory arthritis often have systemic bone loss due to increased bone resorption and decreased bone formation (1). Depletion of NOTCH in mice during embryonic development increased formation of both osteoblasts (10) and osteoclasts (12). We reasoned that NOTCH inhibition may have a different effect on bone mass of TNF-Tg mice compared with these genetically modified mice because MSCs from TNF-Tg mice have abnormally high NOTCH activation. Since persistent NOTCH inhibition (30) or activation (31) have detrimental effects on the skeleton, and high doses of NOTCH inhibitors have severe side effects in vivo, we decided to use low daily doses of DAPT. The half-life of DAPT in vivo is approximately 6 hours (32), and long-term, low-dose DAPT appears to have no notable side effects (28).

To determine whether DAPT prevents inflammatory bone loss, we treated TNF-Tg mice with DAPT or vehicle by daily gavage for 3 months. The efficacy of NOTCH inhibition was confirmed by demonstrating low expression of *Hes1* in popliteal lymph nodes (data not shown). DAPT treatment had no effect on mouse survival or body weight (data not shown). μCT of vertebral bones showed that DAPT treatment significantly increased the bone volume and the trabecular number and thickness and decreased the trabecular spacing compared with vehicle-treated mice (Figure 3A). Increased bone volume in DAPT-treated mice was confirmed by histomorphometric analysis in H&E-stained sections (Figure 3B). Bones from DAPT-treated mice had significantly increased osteoblast and osteoclast numbers on trabecular surfaces (Figure 3B). Calcein double-labeling in undecalcified sections showed that mineralization rate, bone formation rate, and mineral surface/bone surface were all increased in DAPT-treated mice compared with vehicle-treated controls (Figure 3C). In addition, bone volume, osteoblast number, and osteoclast number were increased in long bones from the same DAPT-treated mice (Figure 3D). DAPT treatment did not affect the severity of inflammation or bone erosion in joints of TNF-Tg mice (data not shown).

To determine whether long-term DAPT treatment increased bone formation by increasing MSC osteoblastic differentiation, we cultured BM stromal cells from DAPT- or vehicle-treated mice. Consistent with increased osteoblast-mediated bone formation, cells from DAPT-treated mice formed more CFU-fibroblast (CFU-F) and CFU-ALP$^+$ colonies compared with those from vehicle-treated mice (Figure 3E). mRNA expression of the osteoblast marker genes *Alp* and *Runx2* from CFU-ALP$^+$ colonies was increased in DAPT-treated mice (Figure 3F). We also found a small, but significant, increase in osteoclast formation when BM cells were cultured from DAPT-treated mice (Figure 3G).

Long-term treatment with high doses of DAPT causes damage to organs, including intestine and kidney, which could limit the potential clinical use of this class of reagents (33). Our DAPT regimen did not affect liver, lung, small intestine, or kidney at the microscopic level, nor did it affect body weight or survival (Supplemental Figure 7 and data not shown).

NOTCH inhibition by thapsigargin reverses decreased osteoblast differentiation and prevents bone loss in TNF-Tg mice. To further demonstrate that NOTCH inhibition reverses decreased osteoblast differentiation of MSCs and prevents bone loss in TNF-Tg mice, we used thapsigargin, which has been identified recently as a NOTCH inhibitor via complementary genomic screening (34). Thapsigargin regulates intracellular Ca^{2+} via inhibition of the endoplasmic reticulum in bone cells (35, 36) and interferes with processing of the NOTCH receptor in the endoplasmic reticulum, leading to accumulation of misfolded receptor, which inhibits NOTCH signaling (34). Thapsigargin-derived drugs have been tested in phase I clinical trails for breast, kidney, and prostate cancer (37). Thapsigargin is a much more potent inhibitor of NOTCH signaling than the γ-secretase activity inhibitor DAPT, requiring 0.4 mg/kg/injection (34) compared with 5 mg/kg/injection in vivo (28). However, the effects of thapsigargin on NOTCH signaling in osteoblasts have not previously been studied. We first demonstrated that administration of thapsigargin to TNF-Tg mice decreased *Hes1* mRNA levels in popliteal lymph nodes and CD45$^-$ MSC-enriched cells and also increased CFU-ALP$^+$ colony formation (Supplemental Figure 8, A and B), which suggests that thapsigargin could be used as a new NOTCH inhibitor in our model.

To investigate whether thapsigargin has a bone-anabolic effect in TNF-Tg mice similar to that of DAPT, we treated mice with thapsigargin using both short- and long-term regimens as we did using DAPT (Figures 2 and 3). In vivo bone formation assays using CFU colony cells indicated that cells derived from TNF-Tg mice subjected to short-term thapsigargin treatment (4 days) formed more new bone than cells derived from vehicle-treated mice (Figure 4A). Long-term treatment of TNF-Tg mice with thapsigargin (3 times per week for 2 months) rescued the decreased bone volume and trabecular number, as determined by μCT (Figure 4B).

Histomorphometric analyses confirmed the increased bone volume and osteoblast numbers in thapsigargin-treated mice (Figure 4C). We also tested whether long-term thapsigargin treatment increased bone formation by increasing MSC osteoblastic differentiation. Consistent with increased osteoblast-mediated bone formation, BM cells from thapsigargin-treated mice formed more CFU-F and CFU-ALP$^+$ colonies, which expressed higher levels of osteoblast-related genes and decreased NOTCH target gene levels compared with cells from vehicle-treated mice (Figure 4, D and E, and Supplemental Figure 8C). In this set of experiments, we also treated WT littermates of TNF-Tg mice in parallel to determine whether thapsigargin affects osteoblast function in WT mice. Long-term thapsigargin treatment slightly increased bone volume and osteoblast numbers in WT mice, despite its strong stimulatory effects on osteoblast differentiation in vitro (Figure 4).

The noncanonical NF-κB proteins p52 and RELB mediate TNF-induced NOTCH activation. NF-κB is a major signaling pathway downstream from TNFRs, and it interacts with NOTCH in hematopoietic cells (24). To investigate whether NF-κB proteins participate in TNF-induced NOTCH activation, we examined the expression pattern of *Nfkb* members in our RNA-Seq database. Expression of *Nfkb2* and *Relb*, but not *Nfkb1* or *Rela*, increased in MSCs from TNF-Tg mice (Figure 5A). To confirm this finding, we examined expression of p50, p52, RELA, and RELB proteins in CD45$^-$ MSC-enriched cells from TNF-Tg mice and WT littermates by Western blot. Similar to mRNA levels, expression of RELA and p50 was not markedly changed, but levels of p52, p100, and RELB increased substantially (Figure 5B). DAPT treatment did not affect p52 or RELB levels in CD45$^-$ MSC-enriched cells in WT and TNF-Tg mice, but it rescued the decreased expression of osteoblast-related genes in TNF-Tg cells (Figure 5C), whereas *Hes1* expression was significantly decreased in the same samples (Figure 2B). These data indicate that the change in p52 and RELB levels in MSCs from TNF-Tg mice is unlikely to be due to increased NOTCH activation.

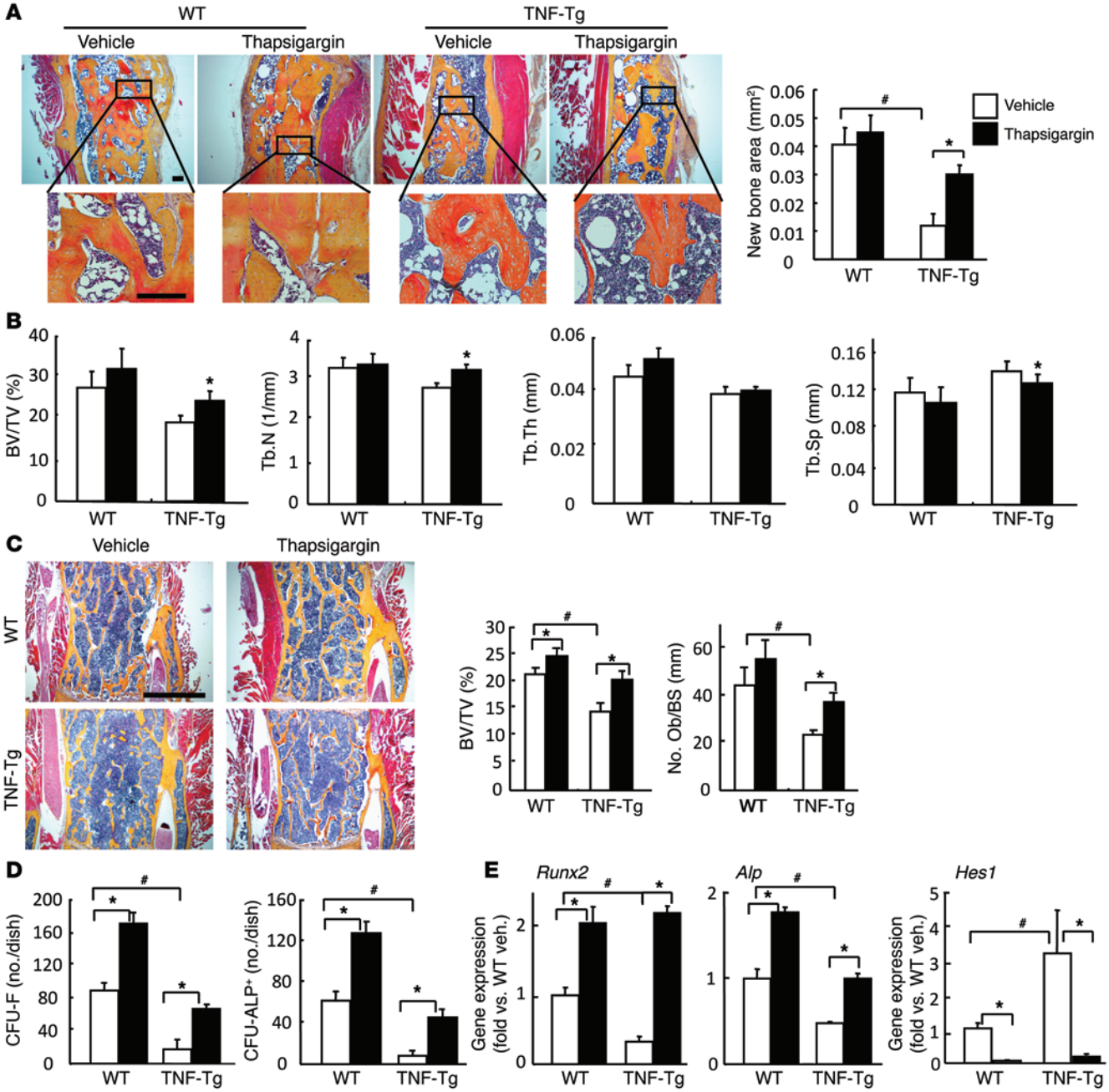

Figure 4

Effects of thapsigargin on osteoblast differentiation and bone volume. (**A**) 2.5-month-old TNF-Tg mice and WT littermates were given thapsigargin (0.4 mg/kg/injection i.p.) or vehicle daily for 4 days. CFU colony cells were derived from the mice and implanted to bone matrix in tibial cortical defects of SCID mice as in Figure 2. Mice were sacrificed 6 weeks after surgery. Shown are histomorphometric analyses and the calculated area of newly formed trabecular bone in decalcified H&E-stained bone sections. $n = 6$ per group. (**B**–**E**) 2.5-month-old TNF-Tg mice and WT littermates were given thapsigargin (0.4 mg/kg/injection i.p.) or vehicle 3 times per week for 2 months. The lumbar vertebrae were subjected to μCT and histological analyses as in Figure 3, and BM cells from long bones were used for biological analyses. $n = 6$ per group. (**B**) Morphometric data from μCT. (**C**) Histology and histomorphometric analysis. (**D**) BM cells were cultured in basal or osteoblast-inducing medium for 21 days in CFU colony formation assays. The number of CFU-F and CFU-ALP⁺ colonies was evaluated. Values are mean ± SD of 4 dishes. (**E**) Expression of osteoblast-related and NOTCH target genes in CFU-F colony cells, determined by qPCR. Scale bars: 100 μm (**A**); 1 mm (**C**). $^{*}P < 0.05$ vs. vehicle; $^{\#}P < 0.05$ vs. WT.

To examine whether p52 and RELB influence NOTCH activation, we overexpressed p52 and RELB in the presence or absence of low-dose NOTCH2-NICD in murine C3H10T1/2 cells with a RBPjκ-Luc reporter construct, which contains 6 RBPjκ response elements in front of the luciferase gene (10). Overexpression of p52 or RELB alone had no effect on RBPjκ-Luc activity, and low-dose NOTCH2-NICD increased RBPjκ-Luc reporter activity 4-fold. Importantly, overexpression of p52 or RELB markedly increased

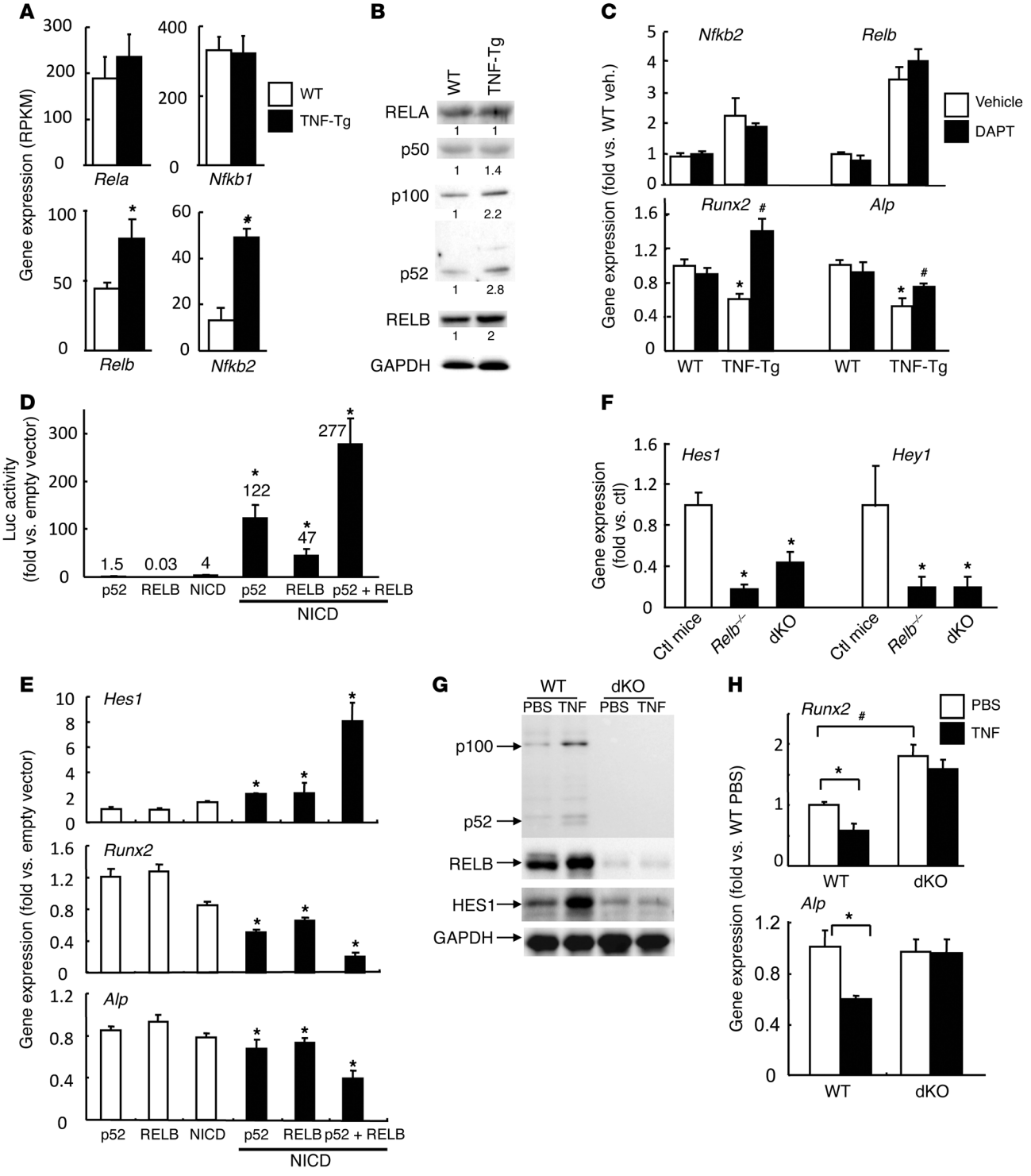

Figure 5

Noncanonical NF-κB proteins p52 and RELB mediate TNF-induced NOTCH activation. (**A**) *Nfkb* mRNA expression in CD45$^-$SCA1$^+$CD105$^+$ MSCs from TNF-Tg mice and WT littermates by RNA-Seq. (**B**) NF-κB protein expression in CD45$^-$ MSC-enriched cells from TNF-Tg mice and WT littermates by Western blot. Fold change in protein level (below) was determined by measuring band intensity. (**C**) *Nfkb2*, *Relb*, *Runx2*, and *Alp* mRNA expression in CD45$^-$ MSC-enriched cells from DAPT- or vehicle-treated TNF-Tg mice by qPCR. (**D**) Reporter activity in C3H10T1/2 cells cotransfected with RBPjκ-Luc and with NOTCH2-NICD–, p52-, and/or RELB-expressing vectors. Fold increase versus empty vector was calculated. (**E**) Expression of *Hes1*, *Runx2*, and *Alp* in cells as in **D**. (**F**) Expression of *Hes1* and *Hey1* in CD45$^-$Ter119$^-$ MSCs from p52/RELB dKO mice, *Relb*$^{-/-}$ mice, and control littermates. Values are mean ± SD of 3 pairs of mice. (**G** and **H**) Bone-derived MSCs of p52/RELB dKO and control littermates were treated with TNF. (**G**) Expression of p52, RELB, and HES1 protein by Western blot. (**H**) Expression of *Runx2* and *Alp* by qPCR. $^*P < 0.05$, $^\#P < 0.05$ vs. control.

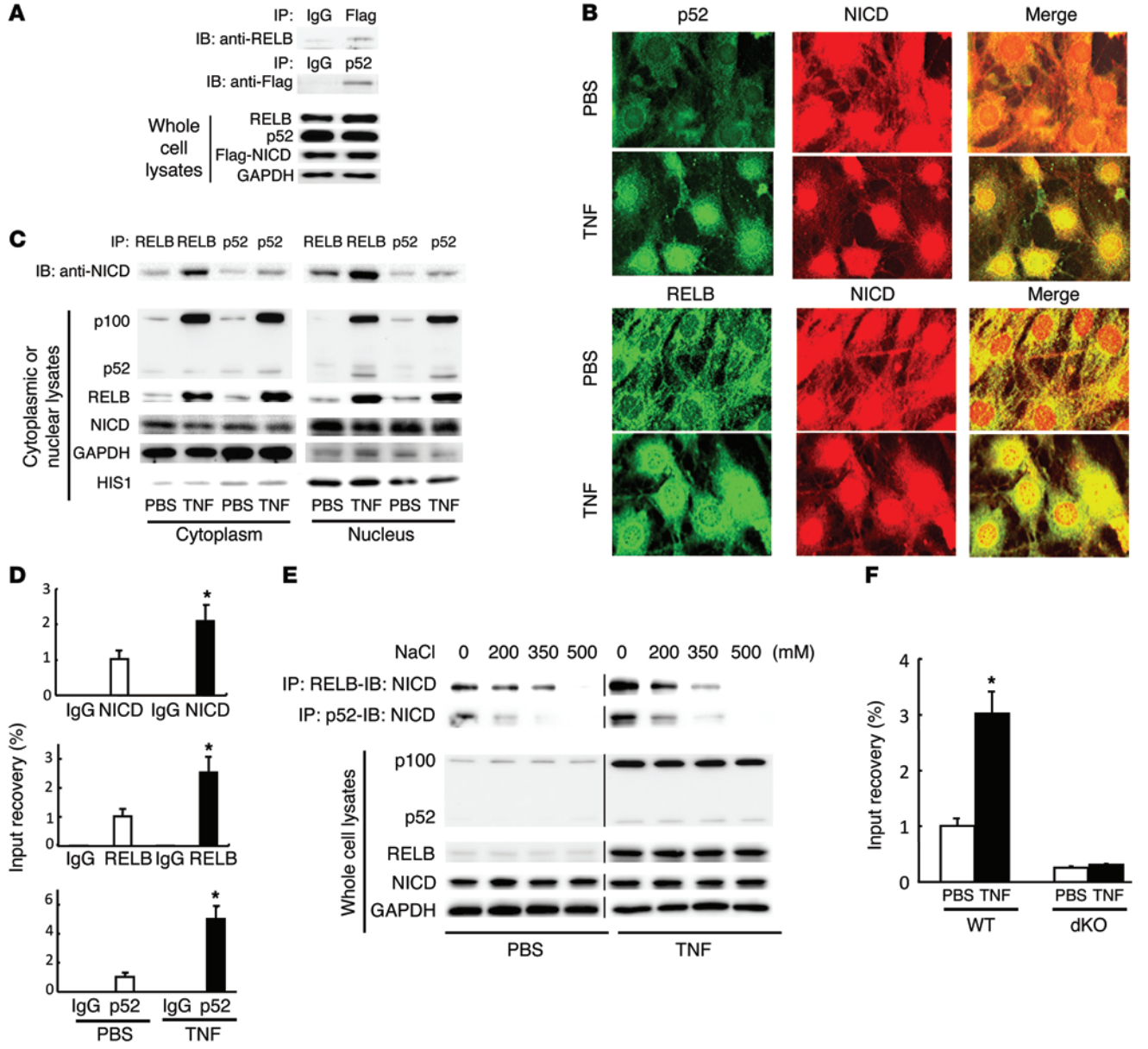

Figure 6

p52 and RELB bind to NICD and are recruited to the *Hes1* promoter. (**A**–**E**) C3H10T1/2 cells were treated with TNF for 24 hours in some experiments. (**A**) Cells were cotransfected with Flag-tagged NOTCH2-NICD, p52, and RELB expression vectors. Whole-cell lysates were subjected to IP with anti-Flag or anti-p52 antibodies and blotted with anti-RELB or anti-Flag antibodies. Experiments were repeated independently 4 times. (**B**) Colocalization of p52 or RELB with NICD was determined by immunofluorescent staining using anti-p52, -RELB, and –NOTCH2-NICD antibodies under confocal microscopy. (**C**) Nuclear and cytoplasm proteins were isolated. Protein lysates were subjected to IP with anti-p52 or anti-RELB antibodies. Immunocomplexes were blotted with anti–NOTCH2-NICD. Expression of p52, RELB and NICD proteins were examined in cytoplasmic and nuclear fractions. Experiments were repeated independently 4 times. (**D**) The ChIP assay was performed on immunocomplex subjected to IP with anti–NOTCH2-NICD, anti-RELB or anti-p52 antibodies. Rat IgG was used as control. Precipitated DNA was measured by qPCR using sequence-specific primers. (**E**) Total protein lysates were subjected to IP with anti-p52 or anti-RELB antibodies. Immunocomplexes were washed with concentration gradient of NaCl, then blotted with anti–NOTCH2-NICD. Experiments were repeated independently 3 times. Lanes were run on the same gel but were noncontiguous. (**F**) Bone-derived MSCs from p52/RELB dKO and WT mice were treated with TNF or PBS and subjected to ChIP as in **E**. Values are mean ± SD of triplicate determinants. **P* < 0.05 vs. respective control.

NOTCH2-NICD–induced RBPjκ-Luc reporter activity, and p52 and RELB combined had a synergistic effect, which was also observed in *Hes1* expression levels when total RNA from transfected cells was used (Figure 5, D and E). Consistent with the notion that NOTCH activation limits osteoblast differentiation, overexpression of p52, RELB, and NICD significantly reduced *Runx2* and *Alp* expression (Figure 5E). To investigate whether p52 and RELB regulate NOTCH signaling, we examined the gene expression lev-

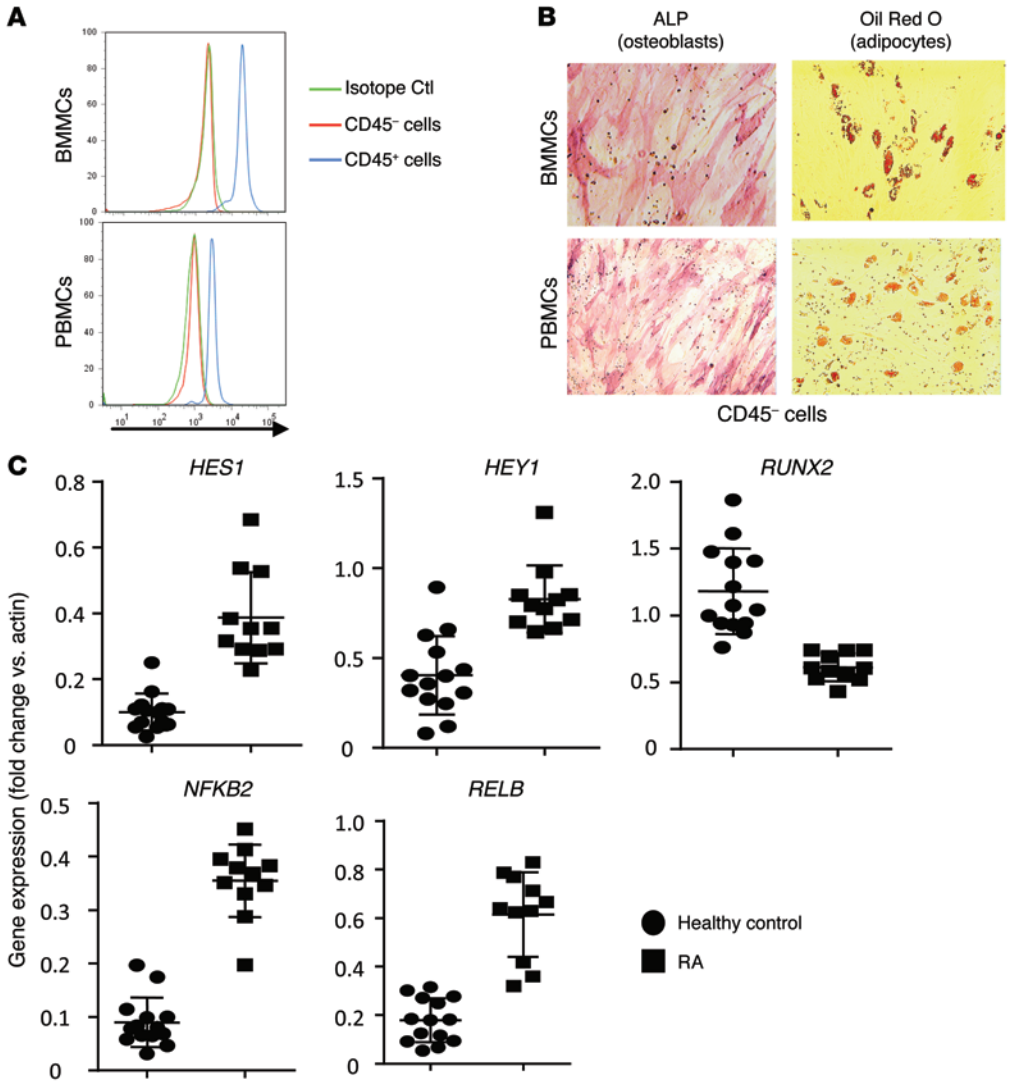

Figure 7
Increased NOTCH activation in CD45⁻ MSC/osteogenic precursors from RA patients. (**A**) CD45⁻ and CD45⁺ cells isolated from human BMMCs and PBMCs were stained with anti-CD45 antibody for FACS analysis. (**B**) CD45⁻ cells isolated from BMMCs and PBMCs were subjected to osteoblast (ALP) and adipocyte (Oil Red O) differentiation assays. Original magnification, ×10. (**C**) Expression levels of NOTCH target genes, *RUNX2*, and noncanonical NF-κB members were measured by qPCR in CD45⁻ cells isolated from PBMCs from healthy control subjects (n = 14) and patients with RA (n = 11). Values were calculated as $Ct_{gene\ of\ interest}/2 - Ct_{actin} \times 100$.

els of *Hes1* and *Hey1* in purified CD45⁻Ter119⁻ MSCs from p52/RELB dKO mice and found that they were reduced (Figure 5F). To determine whether p52 and RELB mediate TNF-induced upregulation of *Hes1*, we treated 3rd-passage bone-derived MSCs from p52/RELB dKO mice and control littermates with TNF. Western blot analysis showed that TNF increased HES1 protein expression in cells from control mice, but not from p52/RELB dKO mice (Figure 5G). qPCR analysis showed that TNF decreased expression of osteoblast-related genes in WT cells, but not in p52/RELB dKO cells (Figure 5H).

p52 and RELB bind to NICD and are recruited to the Hes1 promoter. To examine the molecular mechanism by which p52 and RELB activate NOTCH target gene transcription, we examined whether p52 and RELB bind to NICD, which associates with RBPjκ, the key transcription factor in canonical NOTCH signaling. We transfected C3H10T1/2 cells with Flag-tagged NOTCH2-NICD and with p52 and RELB expression plasmids, performed IP with anti-Flag antibody against NOTCH2-NICD or anti-p52 antibody against p52, and then blotted immunocomplexes with anti-RELB or anti-Flag antibody. Both p52 and RELB bound to NICD (Figure 6A). We hypothesized that TNF enhances the interaction between RELB or p52 and the NICD in MSCs to activate NOTCH signaling. To test this, we cultured C3H10T1/2 cells to confluence; under this culture condition, expression of endogenous NICD was increased due to cell-cell contact–mediated NOTCH activation (Supplemental Figure 9). We treated cells with TNF for 24 hours and examined colocalization of p52, RELB, and NICD by immunofluorescence staining with anti-p52, -RELB, or –NOTCH2-NICD antibodies. As reported previously (38), under basal conditions, RELB and p52 were expressed mainly in the cytoplasm and NICD mainly in the nucleus. After TNF treatment, colocalization of NICD with p52 or RELB increased markedly in the nucleus (Figure 6B). To examine whether TNF increases the interaction of RELB or p52 with NICD and whether this occurs in the cytoplasm or the nucleus, we treated cells with TNF, isolated cytoplasmic or nuclear fractions, performed IP with RELB or p52, and blotted the immunocomplexes with anti–NOTCH2-NICD. TNF increased the total amount of RELB and p100/p52 proteins in both cytoplasmic and nuclear fractions. TNF increased the binding of NICD to RELB and p52 in both the cytoplasm and the nuclei, despite the fact that it decreased the total amount of NICD protein in these compartments (Figure 6C). To determine whether TNF-induced NICD/

RELB or NICD/p52 interaction occurs on the native *Hes1* promoter, we performed ChIP assays using primers that flank the RBPjκ binding sites on the mouse *Hes1* promoter. TNF treatment significantly increased the amount of NICD, p52, and RELB that bound to the RBPjκ binding sites on the *Hes1* promoter (Figure 6D).

To determine whether the increased binding of NICD to RELB and p52 resulted from altered affinity in response to TNF or was due only to increased p52 and RELB expression, we performed an affinity assay (39) by washing the IP complex with gradient NaCl solutions. A high NaCl concentration (500 mM) dissociated the binding of NICD with p52 and RELB in both TNF- and PBS-treated samples (Figure 6E), which suggests that TNF does not affect the binding affinity of NICD for NF-κB proteins. To determine whether TNF increases NICD ChIP without overexpression of p52 or RELB, and whether knockdown of endogenous p52/RELB abolishes this increase, we performed ChIP assays using bone-derived cells from p52/RELB dKO and WT mice. TNF increased the binding of NICD to native RBPjκ binding sites on the *Hes1* promoter in WT cells, which was abolished in p52/RELB dKO cells (Figure 6F).

MSCs from patients with RA have elevated Notch activation. To determine the clinical relevance of our mouse findings, we next examined the expression levels of NOTCH, NF-κB, and osteoblast-related genes in MSCs of RA patients. We first examined properties of $CD45^-$ MSCs isolated from healthy human BM mononuclear cells (BMMCs) and PBMCs. We isolated $CD45^-$ and $CD45^+$ cells using magnetic beads as we did for mouse cells (Figure 1A) and stained them with FITC-conjugated anti-CD45 for fluorescence-activated cell sorting (FACS; Figure 7A). $CD45^-$ cells were cultured in osteoblast- or adipocyte-inducing medium. $CD45^-$ cells from both BMMCs and PBMCs gave rise to osteoblasts and adipocytes (Figure 7B), which indicates that $CD45^-$ cells from PBMCs contain MSC-enriched cells. Using $CD45^-$ MSC-enriched cells from PBMCs of 14 healthy controls and 11 RA patients (active disease, DAS28 score >5, not on bisphosphonates or biologics; see Methods), we measured gene expression levels by qPCR. Similar to our data from TNF-Tg RA mice, expression levels of NOTCH- and NF-κB–regulated genes were significantly increased in $CD45^-$ MSC-enriched cells from RA patients compared with those of healthy controls, whereas *RUNX2* expression levels were markedly decreased (Figure 7C). In addition, $CD45^-$ cells from BMMCs or PBMCs of TNF-Tg mice had similarly increased *Hes1* and decreased *Runx2* RNA expression levels (Supplemental Figure 10). $CD45^-$ PBMCs from RA patients had increased mRNA levels of NOTCH- and NF-κB–regulated genes and decreased *RUNX2* compared with cells from healthy subjects (Figure 7C), which indicates that elevated NOTCH in MSCs likely contributes to reduced osteoblast function in RA patients.

Discussion

Data from various genetically modified mice reveal a complicated role for NOTCH in MSC-osteoblast differentiation, which is tightly regulated both temporally and spatially. For example, NOTCH blocks MSC commitment to the osteoblast lineage when activated in MSCs, although it does not appear to have an important role in committed osteoblasts. Consequently, therapeutic targeting of this pathway is considered to be challenging, and thus the role of NOTCH in common bone diseases has not been studied extensively. Here, using unbiased pathway analysis of RNA-Seq data obtained from purified MSCs after chronic exposure to TNF in vivo, we found an increase in the expression of NOTCH signaling genes. MSCs from TNF-Tg mice, a model of chronic inflammatory arthritis, had significantly decreased osteoblast differentiation. The NOTCH inhibitors DAPT and thapsigargin increased bone volume and osteoblast number and activity in TNF-Tg mice. MSCs from DAPT-treated TNF-Tg mice had increased osteoblast differentiation in in vitro cultures and formed more new bone after injection into recipient mice in vivo. At the molecular level, TNF increased the expression levels of noncanonical NF-κB proteins p52 and RELB, which interacted with NICD on the *Hes1* promoter and upregulated NOTCH target gene expression. Thus, our findings revealed a new role of NOTCH in inflammatory bone loss, such as occurs in RA, in which persistent NOTCH activation in MSCs inhibits their differentiation into osteoblasts.

We speculate that there are 2 fundamental differences between our TNF-Tg mice and genetically modified *Notch* mouse models with respect to NOTCH activation in MSCs. First, in TNF-Tg mice, NOTCH activation resulted from chronic low-level systemic inflammation, rather than being driven by a specific promoter (i.e., NOTCH manipulation occurs only when cells express the promoter). Second, in TNF-Tg mice, the degree of NOTCH activation was low to moderate, which we found to be preventable by NOTCH inhibitor treatment. In contrast, in most animal models, NOTCH activation is persistent because the mice carry a constitutively activated NICD at very high levels that cannot be inhibited by NOTCH inhibitors unless very high doses are used.

NOTCH controls osteoclast function by negatively regulating osteoclastogenesis (40). Osteoclast-specific depletion of RBPjκ increases TNF-induced osteoclast formation (12) and local bone erosion in antibody-induced arthritis (41). The NOTCH/RBPjκ pathway promotes LPS-induced M1 inflammatory macrophage polarization (42), while osteoclasts are derived from M2 housekeeping macrophages (43). These findings suggest that NOTCH/RBPjκ inhibition might favor osteoclastogenesis and bone loss in an inflammatory environment, which appears at odds with the anabolic effect of NOTCH inhibition that we observed herein. In fact, we did observe a small increase in osteoclast numbers in DAPT-treated TNF-Tg mice. However, the overall effect was a significant increase in bone volume in these animals (Figure 3D), which indicates that the bone-anabolic effect of low-dose NOTCH inhibition in this study was greater than the bone-resorptive effects. NOTCH inhibition increases osteoclastogenesis (44), and myeloid-specific deletion of RBPjκ enhances TNF-induced osteoclast formation (41). However, NOTCH activation has been previously reported in synovial samples from RA patients and from mice in animal models of RA (45, 46). NOTCH mediates hypoxia-induced angiogenesis in RA by increasing the function of microvascular endothelial cells (47). Recent studies using DAPT (48) or an anti-mouse Delta-like 1–blocking monoclonal antibody (49) reported that NOTCH inhibition in mice with inflammatory arthritis reduces the severity of inflammation and inhibits osteoclastogenesis. These reports highlight the complexity of NOTCH signaling under normal and pathological conditions. We did not observe reduced joint inflammation in our present study. One potential reason why we did not find changes in inflammation or bone erosion in DAPT-treated mice is that the dose we used was low (5 mg/kg) compared with larger doses used previously (10–20 mg/kg; ref. 48).

Activation of NOTCH signaling is regulated at many levels. For example, TNF regulates NOTCH signaling in several cell types by different mechanisms: it regulates expression of NOTCH ligands (JAG2) and receptors (NOTCH1 and NOTCH4) in fibroblasts,

endothelial cells, and skeletal muscle cells (45, 50, 51) and induces HES1 expression in mouse embryonic fibroblasts (50). Our present results revealed a new molecular mechanism of TNF-induced NOTCH activation in MSCs: TNF activates NOTCH at a step after NICD release. Although TNF-treated cells had reduced NICD expression levels in both cytoplasm and nuclei, they had more NICD binding to the RBPjκ sequence on the *Hes1* promoter (Figure 6, C and D). In this model, the noncanonical NF-κB proteins RELB and p52 potentiated the effect of TNF, and in their absence, TNF-stimulated *Hes1* expression was abolished.

Studies of NOTCH interaction with NF-κB have focused mainly on canonical NF-κB p65 and p50 proteins (25) and how NOTCH regulates *Nfkb* transcription (23–25). We found that NOTCH inhibition did not affect *Nfkb2* expression, but MSCs from p52/RELB dKO mice had significantly reduced expression levels of NOTCH target genes (Figure 5, C and H), which indicates that RELB and p52 work upstream of NOTCH signaling in MSCs. NF-κB consensus sequences could interact with the RBPjκ binding site on target genes (52). However, our findings showed that overexpression of RELB and p52 did not affect RBPjκ-Luc reporter activity or *Hes1* expression, whereas RELB and p52 in combination with NICD significantly increased RBPjκ-Luc reporter activity as well as *Hes1* expression (Figure 5, D and E), which indicates that RELB and p52 need the NICD to regulate NOTCH target gene expression.

We used DAPT, a γ-secretase inhibitor, and thapsigargin, a newly identified NOTCH inhibitor (34), to inhibit NOTCH activation. Several γ-secretase inhibitors have been used in phase II clinical trails in diseases such as Alzheimer's disease (53) and cancer (31). It is unclear whether NOTCH inhibitors can be used to increase bone formation in RA patients; however, data from the genetically modified *Notch* mice demonstrated the complexity of the role of NOTCH in osteoblast differentiation: it functions early to block MSC commitment to the osteoblast lineage, and later promotes osteoblast maturation. Thus, therapeutic targeting of this pathway could be challenging. However, our present data indicated that the NOTCH inhibitor has a clearly beneficial bone-anabolic effect in an experimental model of RA in which NOTCH signaling is already elevated. A recent study demonstrated that osteoblasts are short-lived, nonreplicative cells, requiring continual replenishment from BM MSCs (54). Thus, if NOTCH signaling is elevated persistently in MSCs in RA patients, it will decrease the osteoblast pool by blocking the MSC-osteoblast transition and thereby inhibit bone formation. Under these conditions, NOTCH inhibition could lift this blockage to increase osteoblast numbers and thus bone volume. Our data showed that $CD45^-$ MSC-enriched cells from RA patients expressed increased levels of *HES1* and *HEY1* and decreased levels of *RUNX2* compared with those from healthy subjects, which indicates that the elevated NOTCH signaling in MSCs in RA mice likely occurs in human RA patients as well. Since patients with other types of chronic inflammatory diseases — such as systemic lupus erythematosus and Crohn's disease — often have systemic bone loss, it is possible that they also have abnormal NOTCH activation in their MSCs that contributes to reduced osteoblast function.

In summary, using TNF-Tg mice as a model of RA, we demonstrated that chronic inflammation caused persistent activation of the NOTCH pathway in MSCs, limiting their osteoblast differentiation, which was prevented by administration of a NOTCH inhibitor. At the molecular level, we found that inflammation increased the expression of noncanonical NF-κB proteins, which potentiated NOTCH activation by binding to and promoting nuclear translocation of NICD. Thus, NOTCH inhibition represents a potential new therapy for inflammation-induced bone loss associated with NOTCH activation in MSCs.

Methods

Reagents and animals. DAPT was from Calbiochem and thapsigargin was purchased from ENZO life sciences. M-CSF, RANKL, and TNF for cell culture were purchased from R&D Systems. TNF-Tg mice (line 3647), originally obtained from G. Kollias (Biomedical Sciences Research Centre "Alexander Fleming," Vari, Greece), carry a 3′-modified human *TNF* transgene in which the 3′-region of the *TNF* gene was replaced with that of the human β-globin gene. These mice develop arthritis starting at 2 months of age, and arthritis and bone loss progress with age. TNF-Tg 3647 mice can survive to 1 year or older, unlike the commonly used TNF-Tg 197 mice, which develop more severe arthritis and die within a few months of birth. We consider the chronic nature of the disease in TNF-Tg 3647 mice to be advantageous because it is more closely mimics human RA. *Nfkb2*$^{-/-}$ mice, and mice with a mutation-disrupted *Relb* locus by random integration of transgene sequences, have been described previously (21, 55). *Nfkb2*$^{+/-}$ *Relb*$^{+/-}$ mice were crossed with *Nfkb2*$^{-/-}$ *Relb*$^{+/-}$ mice to generate *Nfkb2*$^{-/-}$ *Relb*$^{-/-}$ mice (p52/RELB dKO). The mice used were in a mixed 129 and C57BL/6J background. *Tnfr1*$^{-/-}$ *Tnfr2*$^{-/-}$ mice (TNFR1/2 dKO) in a C57BL/6J background were provided by G.S. Pryhuber (Department of Pediatrics, University of Rochester School of Medicine and Dentistry, Rochester, New York, USA; ref. 56). Transplant recipients were 2-month-old SCID mice (strain B6.CB17-Prkdcscid/SzJ; stock no. 001913; Jackson Laboratories). *Rosa26-LacZ* mice (strain B6;129S-Gt[ROSA]26Sor/J; stock no. 002073; Jackson Laboratories) were used in in vivo tracking experiments.

MSC preparation. We used several types of cell preparations as MSCs and MSC-enriched cells based on individual experimental needs.

For FACS-sorted purified MSCs, we used the following antibodies (from eBioscience and BD Biosciences — Pharmingen): CD45, SCA1, CD105, Ter119. Whole BM cells were incubated with anti-CD45 antibody–conjugated microbeads (Miltenyi Biotec). The $CD45^-$ population was isolated by negative selection according to the manufacturer's instructions. $CD45^-$ cells were stained with a combination of SCA1 and CD105. $CD45^-SCA1^+CD105^+$ cells were isolated by FACS sorting and used in RNA-Seq and qPCR.

$CD45^-$ MSC-enriched cells were isolated by negative selection, as described above. We previously reported that $CD45^-$ cells express MSCs surface markers and can differentiate into multiple lineages (1). $CD45^-$ cells were used in qPCR and Western blot analysis.

Mesenchymal colony cells, generated by pooling cells from CFU colonies, were used for in vivo bone formation assays.

Bone-derived MSCs were isolated using a recently published protocol (57). Long bones were flushed several times with PBS, cut into small pieces, and cultured in a plastic dish for 3 days. The bone pieces were transferred into a clear dish as 1st-passage cells and continually cultured for another 7 days to allow the cells to become confluent. 3rd-passage cells were used for cell characterization and experiments. The MSC characteristics of bone-derived MSCs were confirmed by FACS and multilineage differentiation assays (Supplemental Figure 1). Bone-derived MSCs were used for Western blot and IP.

The C3H10T1/2 mouse MSC cell line was used in experiments involving transient transfection, Western blot, and ChIP assays.

Human MSCs (catalog no. PT-2501; Lonza) were used in qPCR analyses.

RNA-Seq and IPA. $CD45^-SCA1^+CD105^+$ MSCs were isolated from TNF-Tg mice and WT littermates. Cells (1×10^4) were subjected to mRNA isolation and RNA-Seq with SOLiD system (Applied Biosystems). Pathway analysis of statistically significant gene expression changes from mRNA sequenc-

ing was performed with IPA (Ingenuity System) and David Bioinformatics Resources program (Visualization and Integrated Discovery; http://david.abcc.ncifcrf.gov/home.jsp; ref. 58). Genes from the mRNA sequencing data set that met the 1.5-fold ($P < 0.05$) change cutoff and were associated with biological functions in the Ingenuity Pathways Knowledge Base or KEGG database were considered for analysis. For all analyses, Fisher exact test was used to calculate a P value determining the probability that each signal pathway assigned to that data set was due to chance alone. RNA-Seq data were deposited in the NCBI Sequence Read Archive (http://www.ncbi.nlm.nih.gov/sra; accession no. SRX543086).

Cell culture and analysis. For CFU-F and CFU-ALP assays, total BM cells were cultured in 10-cm dishes at 10^6 cells/dish in 10 ml α-MEM containing 10% FCS (Hyclone Laboratories) with or without 50 μg/ml ascorbic acid and 10 mM β-glycerophosphate for 28 days. At the end of the culture period, cells were stained for CFU-F or CFU-ALP activity. The stained CFU-F and CFU-AFP$^+$ colonies were counted (>20 cells in a single colony). For osteoclastogenic assays, BM cells were cultured with conditioned medium (1:50 dilution) from a M-CSF–producing cell line for 3 days in α-MEM with 10% FCS to enrich for osteoclast precursors. Osteoclast precursors were cultured with M-CSF conditioned medium and RANKL (10 ng/ml, R&D) for 2–3 days. After multinucleated cells were observed under a microscope, the cells were fixed, stained for TRAP activity to identify osteoclasts (TRAP$^+$ cells containing >3 nuclei), and counted, as described previously (55). For differentiation assay of human CD45$^-$ cells, PBMCs and BMMCs were cultured in 60-mm dishes at 2×10^6 cells/dish in 4 ml α-MEM culture medium containing 10% FCS with 50 μg/ml ascorbic acid and 10 mM β-glycerophosphate for osteoblast induction, or containing 10% FCS, 10 nM dexamethasone, 5 μg/ml insulin (Sigma-Aldrich), 100 nM indomethacin (Sigma-Aldrich), and 0.5 mM methylisobutylxanthine (Sigma-Aldrich) for adipocyte induction. Cells were stained for ALP activity for osteoblasts or with Oil Red for adipocytes.

qPCR. Total RNA was extracted from cell cultures using TRIzol reagent (Invitrogen). cDNAs were synthesized by iSCRIPT cDNA Synthesis Kit (Bio-Rad). qPCR amplifications were performed in an iCycler (Bio-Rad) real-time PCR machine using iQ SYBR Green supermix (Bio-Rad) according to the manufacturer's instructions. *Gapdh* was amplified on the same plates and used to normalize the data. Samples were prepared in triplicate, and each experiment was repeated at least 3 times. The relative abundance of each gene was calculated by subtracting the Ct value of each sample for an individual gene from the corresponding Ct value of *Gapdh* (ΔCt); ΔΔCt was obtained by subtracting the ΔCt of the reference point; and $2^{\Delta\Delta Ct}$ was then calculated to yield fold expression relative to the reference point. Representative data are presented as mean ± SD of the triplicates or of 4 wells of cell culture. See Supplemental Table 1 for sequence-specific primers.

μCT, histology, and histomorphometric analysis of bone sections. For μCT, lumbar 1 (L1) vertebrae and femora were dissected free of soft tissue, fixed overnight in 70% ethanol, and scanned at high resolution (10.5 μm) on a VivaCT40 μCT scanner (Scanco Medical) using 300 ms integration time, 55 kVp energy, and 145 uA intensity. 3D images were generated using a constant threshold of 275 for all samples. For histology and analysis, thoracic vertebrae and tibiae were removed from mice after sacrifice, fixed in 10% buffered formalin, decalcified in 10% EDTA, and embedded in paraffin. Sections (4 μm thick) were then stained with H&E and for TRAP activity. Histomorphometric analysis of osteoclast numbers and osteoblast numbers, expressed per millimeter bone surface in the vertebrae and tibiae, was carried out using an Osteometrics image analysis software system. Calcein double-labeling was performed by i.p. injection of calcein (10 mg/g body weight; C-0875; Sigma-Aldrich) at 6 and 1 days prior to sacrifice, as described previously (59). Bones were harvested and embedded in LR White acrylic resin. Serial sections were cut, and the freshly cut surface of each section was viewed and imaged using fluorescence microscopy. The calcein double-labeled morphometric analysis in trabecular bone was performed using Osteometrics image analysis software. The mineral apposition rate, bone formation rate, and double label surface/bone surface ratio were calculated as we previously described (1).

Confocal microscopy. Cells were treated with TNF for 24 hours, fixed with 4% paraformaldehyde, pretreated with 1% Triton X-100 and 0.5% BSA in PBST, and blocked in 10% BSA in PBST for 30 minutes at RT. Cells were immunostained with anti-NICD, anti-p52, or anti-RELB antibodies at 4°C overnight, incubated with secondary antibodies conjugated with Alexa Fluor 488 and Alexa Fluor 546 for 45 minutes at 37°C, and subjected to confocal microscopy. Confocal images were obtained with a MRC1024 confocal microscope (Bio-Rad). Laser beams with 488- and 543-nm excitation wavelengths were used for DAPI, FITC, and Cy5 imaging. Single confocal images were processed in Adobe Photoshop.

Transfection and luciferase reporter assay. Transient transfection was performed with Lipofectamine (Roche). 1×10^4 C3H10T1/2 cells were seeded in 24-well plates and cotransfected with NOTCH2-NICD (0.05 μg), p52, and/or RELB expressing constructs or the corresponding empty vectors along with RBPjκ-Luc (0.5 μg) and pRL-renilla (0.01 μg; Promega). Cells were cultured for a further 48 hours followed by harvesting for dual luciferase activity assays (Promega) according to the manufacturer's instruction. RBPjκ-Luc reporter activity was defined as the ratio of Firefly/Renilla luciferase activities.

IP and Western blot. For IP, C3H10T1/2 cells were seeded in 10-cm dishes and cotransfected with NICD, p52, or RELB expression vectors for 24 hours. Proteins from cell lysates were quantitated using a kit from Bio-Rad and subjected to IP as described in the technical bulletin from Sigma-Aldrich. Briefly, 300 μg of proteins in 1 ml cell lysis buffer were added with 1 μg antibody and incubated for 1 hour at 4°C, then incubated with prewashed EZview Red Protein A/G Affinity Gel beads (Sigma-Aldrich) for another hour at 4°C. To test whether TNF affected the binding affinity of NF-κB and NICD proteins, we performed an affinity assay according to a published protocol (39). In brief, the IP complex was washed 3 times with gradient concentrations of NaCl wash buffer containing 0, 200, 350, or 500 mM NaCl for 15 minutes. Eluted samples were fractionated by SDS-PAGE and transferred to PVDF membranes. For Western blot analysis, whole-cell lysates (10 μg) were loaded in 10% SDS-PAGE gels and blotted with antibodies against HES1, p52, RELB, p50, RELA (Santa Cruz Biotechnology Inc.) and NOTCH2-NICD (Developmental Studies Hybridoma Bank, University of Iowa) or mouse GAPDH (Santa Cruz Biotechnology Inc.).

ChIP. C3H10T1/2 cells and 3rd-passage bone-derived cells from WT and p52/RELB dKO mice were treated with TNF for 24 hours after reaching confluence. ChIP was performed with MAGnify Chromatin Immunoprecipitation System (Invitrogen) according to the manufacturer's instructions. A total of 3×10^6 C3H10T1/2 cells was used for each experiment. Cells were treated with 1% formaldehyde for 15 minutes and then sonicated on ice 16 times (30 seconds on, 30 seconds off) at high power using a Bioruptor UCD-200 sonicator. Antibodies against NOTCH2-NICD, RELB (Santa Cruz Biotechnology Inc.), or p52 (Cell Signaling Technology) and control rat IgG (Invitrogen) were used with 100 μg chromatin per ChIP procedure. The amounts of each specific DNA fragment in IPs were determined by qPCR. Primers used for this analysis were as follows: RBPjκ, –194 to +160, 5′-CTCAGGCGCGCGCCATTGGCC-3′ (forward), 5′-GCTTACGTCCTTTTACTTGAC-3′ (reverse); negative control, 1.5 kb downstream from the RBPjκ binding sites of the *Hes1* promoter, 5′-CCTAGGGAGAAGGAGCTGGCT-3′ (forward), 5′-TGGCCGTCAGGAGCCGGCACC-3′ (reverse).

Tibial bone defect model. 2 month-old SCID mice ($n = 4$) were anesthetized, and bilateral 2 × 5 mm cortical bone defects were made in the anterior proximal tibiae and filled with bovine bone matrix. 5×10^5 cells from mesenchymal colony cells were injected into the bone matrix in defects. The right tibiae received cells from vehicle-treated mice and the left tibiae received cells from

DAPT-treated mice. Mice were sacrificed 6 weeks after surgery, and the volume of new bone formed in the defects (expressed as a percentage of the total defect volume) was measured by μCT, followed by histomorphometric analysis of the area of newly formed trabecular bone and associated spindle-shaped fibroblast-like cells observed in decalcified H&E-stained bone sections.

Patients and sampling. Patients (n = 11) met ACR criteria for RA, were seropositive (CCP^+), had a mean age of 56 years, mean disease duration of 3.25 years, and evidence of disease activity based on the presence of swollen and tender joints. Disease activity was measured by DAS28 scores (mean, 3.5; range, 2.19 to 5.85). Patients on biologics were excluded. Healthy controls (n = 14) were age matched, and subjects on bisphosphonates were excluded. BMMCs and PBMCs were isolated from heparinized BM aspirate and heparinized PB by Ficoll-Hypaque density gradient centrifugation (Pharmacia Biotech) (60, 61). PBMCs and BMMCs were incubated with anti-human CD45 antibody–conjugated microbeads (Miltenyi Biotec). $CD45^-$ and $CD45^+$ populations were collected according to the manufacturer's instructions.

Statistics. All results are given as mean ± SD. Comparisons between 2 groups were analyzed using 2-tailed unpaired Student's t test. 1-way ANOVA and Dunnett's post-hoc multiple comparisons were used for comparisons among 3 or more groups. P values less than 0.05 were considered statistically significant.

Study approval. All animal experiments were performed according to protocols approved by the University of Rochester Medical Center IACUC and conformed to the NIH *Guide for the Care and Use of Laboratory Animals*. For human studies, detailed written informed consent was obtained from all patients and healthy donors, in accordance with protocols approved by the Human Subjects IRB of the University of Rochester Medical Center (RSRB 29181 and 24888).

Acknowledgments

We thank G.S. Pryhuber for providing TNFR1/2 KO mice and Jixiang Shi and Lei Shu for histological analysis. This work was supported by NIH PHS awards AR48697 and AR63650 (to L. Xing); AR43510 (to B.F. Boyce); AR63071 (to M.J. Hilton); and AI077674, P01AI078907, and U19AI56390 (to J.H. Anolik). μCT was supported by NIH grant P30AR0613007. X. Li's salary was supported by a research grant from the National Natural Science Foundation of China (81202037 to Z. Wang).

Received for publication January 22, 2013, and accepted in revised form April 10, 2014.

Address correspondence to: Lianping Xing, Department of Pathology and Laboratory Medicine, 601 Elmwood Ave, Box 626, Rochester, New York 14642, USA. Phone: 585.273.4090; Fax: 585.756.4468; E-mail: Lianping_xing@urmc.rochester.edu.

1. Zhao L, et al. Tumor necrosis factor inhibits mesenchymal stem cell differentiation into osteoblasts via the ubiquitin E3 ligase Wwp1. *Stem Cells*. 2011;29(10):1601–1610.
2. Kaneki H, et al. Tumor necrosis factor promotes Runx2 degradation through up-regulation of Smurf1 and Smurf2 in osteoblasts. *J Biol Chem*. 2006; 281(7):4326–4333.
3. Guo R, et al. Ubiquitin ligase Smurf1 mediates tumor necrosis factor-induced systemic bone loss by promoting proteasomal degradation of bone morphogenetic signaling proteins. *J Biol Chem*. 2008; 283(34):23084–23092.
4. Li P, et al. Systemic tumor necrosis factor alpha mediates an increase in peripheral CD11bhigh osteoclast precursors in tumor necrosis factor alpha-transgenic mice. *Arthritis Rheum*. 2004; 50(1):265–276.
5. Diarra D, et al. Dickkopf-1 is a master regulator of joint remodeling. *Nat Med*. 2007;13(2):156–163.
6. Mukai T, et al. TNF-α inhibits BMP-induced osteoblast differentiation through activating SAPK/JNK signaling. *Biochem Biophys Res Commun*. 2007; 356(4):1004–1010.
7. Li P, Schwarz EM. The TNF-α transgenic mouse model of inflammatory arthritis. *Springer Semin Immunopathol*. 2003;25(1):19–33.
8. Zanotti S, Canalis E. Notch and the skeleton. *Mol Cell Biol*. 2010;30(4):886–896.
9. Engin F, et al. Dimorphic effects of Notch signaling in bone homeostasis. *Nat Med*. 2008;14(3):299–305.
10. Hilton MJ, et al. Notch signaling maintains bone marrow mesenchymal progenitors by suppressing osteoblast differentiation. *Nat Med*. 2008; 14(3):306–314.
11. Zanotti S, Smerdel-Ramoya A, Stadmeyer L, Durant D, Radtke F, Canalis E. Notch inhibits osteoblast differentiation and causes osteopenia. *Endocrinology*. 2008;149(8):3890–3899.
12. Zhao B, et al. Interferon regulatory factor-8 regulates bone metabolism by suppressing osteoclastogenesis. *Nat Med*. 2009;15(9):1066–1071.
13. Karin M, Greten FR. NF-κB: linking inflammation and immunity to cancer development and progression. *Nat Rev Immunol*. 2005;5(10):749–759.
14. Courtois G, Gilmore TD. Mutations in the NF-κB signaling pathway: implications for human disease. *Oncogene*. 2006;25(51):6831–6843.
15. Boyce BF, Yao Z, Xing L. Functions of nuclear factor κB in bone. *Ann N Y Acad Sci*. 2010;1192:367–375.
16. Beg AA, Sha WC, Bronson RT, Ghosh S, Baltimore D. Embryonic lethality and liver degeneration in mice lacking the RelA component of NF-κB. *Nature*. 1995;376(6536):167–170.
17. Vaira S, Alhawagri M, Anwisye I, Kitaura H, Faccio R, Novack DV. RelA/p65 promotes osteoclast differentiation by blocking a RANKL-induced apoptotic JNK pathway in mice. *J Clin Invest*. 2008; 118(6):2088–2097.
18. Chang J, et al. Inhibition of osteoblastic bone formation by nuclear factor-κB. *Nat Med*. 2009; 15(6):682–689.
19. Franzoso G, et al. Requirement for NF-κB in osteoclast and B-cell development. *Genes Dev*. 1997; 11(24):3482–3496.
20. Soysa NS, et al. The pivotal role of the alternative NF-κB pathway in maintenance of basal bone homeostasis and osteoclastogenesis. *J Bone Miner Res*. 2010;25(4):809–818.
21. Zhao C, et al. Noncanonical NF-κB signaling regulates hematopoietic stem cell self-renewal and microenvironment interactions. *Stem Cells*. 2012; 30(4):709–718.
22. Yao Z, Li Y, Yin X, Dong Y, Xing L, Boyce BF. NF-κB RelB negatively regulates osteoblast differentiation and bone formation. *J Bone Miner Res*. 2014; 29(4):866–877.
23. Osipo C, Golde TE, Osborne BA, Miele LA. Off the beaten pathway: the complex cross talk between Notch and NF-κB. *Lab Invest*. 2008;88(1):11–17.
24. Schwarzer R, Jundt F. Notch and NF-κB signaling pathways in the biology of classical Hodgkin lymphoma. *Curr Mol Med*. 2011;11(3):236–245.
25. Maniati E, et al. Crosstalk between the canonical NF-κB and Notch signaling pathways inhibits Pparγ expression and promotes pancreatic cancer progression in mice. *J Clin Invest*. 2011; 121(12):4685–4699.
26. Hansson EM, Lendahl U, Chapman G. Notch signaling in development and disease. *Semin Cancer Biol*. 2004;14(5):320–328.
27. Wright TW, Pryhuber GS, Chess PR, Wang Z, Notter RH, Gigliotti F. TNF receptor signaling contributes to chemokine secretion, inflammation, and respiratory deficits during Pneumocystis pneumonia. *J Immunol*. 2004;172(4):2511–2521.
28. Teachey DT, et al. Targeting Notch signaling in autoimmune and lymphoproliferative disease. *Blood*. 2008;111(2):705–714.
29. Zhang H, Xing L. Ubiquitin E3 ligase Itch negatively regulates osteoblast differentiation from mesenchymal progenitor cells. *Stem Cells*. 2013; 31(8):1574–1583.
30. Geling A, Steiner H, Willem M, Bally-Cuif L, Haass C. A γ-secretase inhibitor blocks Notch signaling in vivo and causes a severe neurogenic phenotype in zebrafish. *EMBO Rep*. 2002;3(7):688–694.
31. Shih Ie M, Wang TL. Notch signaling, γ-secretase inhibitors, and cancer therapy. *Cancer Res*. 2007; 67(5):1879–1882.
32. Tsao PN, et al. Lipopolysaccharide-induced Notch signaling activation through JNK-dependent pathway regulates inflammatory response. *J Biomed Sci*. 2011;18:56.
33. Wu W, Zhang L. γ-Secretase inhibitors for the treatment of Alzheimer's disease. *Drug Develop Res*. 2009; 70(2):94–100.
34. Roti G, et al. Complementary genomic screens identify SERCA as a therapeutic target in NOTCH1 mutated cancer. *Cancer Cell*. 2013;23(3):390–405.
35. Ishihara Y, et al. In situ imaging of the autonomous intracellular Ca(2+) oscillations of osteoblasts and osteocytes in bone. *Bone*. 2012;50(4):842–852.
36. Yip KH, et al. Thapsigargin modulates osteoclastogenesis through the regulation of RANKL-induced signaling pathways and reactive oxygen species production. *J Bone Miner Res*. 2005; 20(8):1462–1471.
37. Ghantous A, Gali-Muhtasib H, Vuorela H, Saliba NA, Darwiche N. What made sesquiterpene lactones reach cancer clinical trials? *Drug Discov Today*. 2010;15(15–16):668–678.
38. Sun SC. Non-canonical NF-κB signaling pathway. *Cell Res*. 2011;21(1):71–85.
39. Sumara I, Vorlaufer E, Gieffers C, Peters BH, Peters JM. Characterization of vertebrate cohesin complexes and their regulation in prophase. *J Cell Biol*. 2000; 151(4):749–762.
40. Duan L, Ren Y. Role of notch signaling in osteoimmunology — from the standpoint of osteoclast differentiation. *Eur J Orthod*. 2013;35(2):175–182.

41. Zhao B, Grimes SN, Li S, Hu X, Ivashkiv LB. TNF-induced osteoclastogenesis and inflammatory bone resorption are inhibited by transcription factor RBP-J. *J Exp Med*. 2012;209(2):319–334.
42. Xu H, et al. Notch-RBP-J signaling regulates the transcription factor IRF8 to promote inflammatory macrophage polarization. *Nat Immunol*. 2012; 13(7):642–650.
43. Brownlow N, Mol C, Hayford C, Ghaem-Maghami S, Dibb NJ. Dasatinib is a potent inhibitor of tumour-associated macrophages, osteoclasts and the FMS receptor. *Leukemia*. 2009;23(3):590–594.
44. Bai S, et al. NOTCH1 regulates osteoclastogenesis directly in osteoclast precursors and indirectly via osteoblast lineage cells. *J Biol Chem*. 2008; 283(10):6509–6518.
45. Ando K, et al. Induction of Notch signaling by tumor necrosis factor in rheumatoid synovial fibroblasts. *Oncogene*. 2003;22(49):7796–7803.
46. Okamoto T. The epigenetic alteration of synovial cell gene expression in rheumatoid arthritis and the roles of nuclear factor κB and Notch signaling pathways. *Mod Rheumatol*. 2005;15(2):79–86.
47. Gao W, et al. Notch-1 mediates hypoxia-induced angiogenesis in rheumatoid arthritis. *Arthritis Rheum*. 2012;64(7):2104–2113.
48. Park JS, et al. Inhibition of Notch signalling ameliorates experimental inflammatory arthritis [published online ahead of print November 19, 2013]. *Ann Rheum Dis*. doi:10.1136/annrheumdis-2013-203467.
49. Sekine C, Koyanagi A, Koyama N, Hozumi K, Chiba S, Yagita H. Differential regulation of osteoclastogenesis by Notch2/Delta-like 1 and Notch1/Jagged1 axes. *Arthritis Res Ther*. 2012;14(2):R45.
50. Fernandez L, et al. Tumor necrosis factor-α and endothelial cells modulate Notch signaling in the bone marrow microenvironment during inflammation. *Exp Hematol*. 2008;36(5):545–558.
51. Acharyya S, et al. TNF inhibits Notch-1 in skeletal muscle cells by Ezh2 and DNA methylation mediated repression: implications in duchenne muscular dystrophy. *PLoS One*. 2010;5(8):e12479.
52. Tao J, Chen S, Lee B. Alteration of Notch signaling in skeletal development and disease. *Ann N Y Acad Sci*. 2010;1192:257–268.
53. Zetterberg H, Mattsson N, Blennow K, Olsson B. Use of theragnostic markers to select drugs for phase II/III trials for Alzheimer disease. *Alzheimers Res Ther*. 2010;2(6):32.
54. Park D, et al. Endogenous bone marrow MSCs are dynamic, fate-restricted participants in bone maintenance and regeneration. *Cell Stem Cell*. 2012; 10(3):259–272.
55. Yao Z, Xing L, Boyce BF. NF-κB p100 limits TNF-induced bone resorption in mice by a TRAF3-dependent mechanism. *J Clin Invest*. 2009; 119(10):3024–3034.
56. Pryhuber GS, et al. Parenchymal cell TNF receptors contribute to inflammatory cell recruitment and respiratory failure in Pneumocystis carinii-induced pneumonia. *J Immunol*. 2008;181(2):1409–1419.
57. Zhu H, et al. A protocol for isolation and culture of mesenchymal stem cells from mouse compact bone. *Nat Protoc*. 2010;5(3):550–560.
58. Majeti R, et al. Dysregulated gene expression networks in human acute myelogenous leukemia stem cells. *Proc Natl Acad Sci U S A*. 2009; 106(9):3396–3401.
59. Zhang HW, et al. Defects in mesenchymal stem cell self-renewal and cell fate determination lead to an osteopenic phenotype in Bmi-1 null mice. *J Bone Miner Res*. 2010;25(3):640–652.
60. Kobie JJ, et al. Decreased influenza-specific B cell responses in rheumatoid arthritis patients treated with anti-tumor necrosis factor. *Arthritis Res Ther*. 2011;13(6):R209.
61. Palanichamy A, et al. Neutrophil-mediated IFN activation in the bone marrow alters B cell development in human and murine systemic lupus erythematosus. *J Immunol*. 2014;192(3):906–918.